Batteries & Supercaps

Research Article
doi.org/10.1002/batt.202300309

Chemistry Europe
European Chemical Societies Publishing

www.batteries-supercaps.org

High-Rate Discharge Minimizes Volume Expansion of Lithium Metal Electrodes under Lean Electrolyte and High Areal Capacity Conditions

Arghya Dutta,*[a] Emiko Mizuki,[a, b] and Shoichi Matsuda*[a, b, c]

The demand for practical implementation of lithium metal batteries (LMBs) is increasing due to their superior energy density. However, poor cycle life and safety concerns regarding dendrite formation remain significant challenges. Recent studies have shown empirical improvements in cycle life through the use of high-rate discharge protocols, but the precise mechanism behind this enhancement is still unclear due to difficulties in analyzing the lithium electrode, especially in LMB cells with high energy density designs. In this study, X-ray computed tomography (XCT) analysis, a non-destructive technique, was employed to investigate the lithium metal electrode in pouch-type cells with a cell-level energy density exceeding 350 Wh kg^{-1}. XCT analysis revealed significant volume expansion of the lithium electrode during charge/discharge cycles, particularly under high-rate charging conditions, which promoted dendritic growth due to inhomogeneous current distribution. However, such undesired volume expansion was largely suppressed during high-rate discharge, leading to improved cycle life. This study underscores the importance of non-destructive techniques in comprehending the degradation mechanisms of high-energy-density LMBs.

Introduction

The continuous progress of conventional lithium-ion battery (LIB) technology over the past three decades has been undeniably successful. However, further enhancements in energy density necessitate the incorporation of high-capacity and high-voltage electrode materials.[1–4] The lithium metal based rechargeable batteries (LMBs) with the use of high-nickel-content lithium nickel manganese cobalt oxide ($LiNi_{0.8}Mn_{0.1}Co_{0.1}O_2$ or NMC811; specific capacity > 220 mAh g^{-1}) as the positive electrode materials, is one of the promising candidates for next-generation high energy density energy storage devices. Despite recent successful demonstrations of LMBs achieving cell-level energy densities above 350 Wh kg^{-1}, there are still significant challenges preventing their widespread commercialization.[5,6] These challenges include poor cycle life (less than 200 cycles), low charging rates (below 0.5 C), and safety concerns related to dendrite formation.[7] To enable the practical implementation of high-energy-density LMBs, it is imperative to develop a comprehensive understanding of the degradation mechanisms affecting Li metal electrodes and to devise effective strategies to address these issues.

In recent years, significant research efforts have focused on the stabilization of Li metal electrode, employing various strategies such as novel electrolyte compositions, artificial solid-electrolyte interphase (SEI) layers, and precise control of stack pressure.[8–16] These studies have made notable progress in enhancing the cycle life of LMBs. In particular, several investigations have empirically demonstrated the improvement of cycle life in LMBs by adopting a relatively higher-rate discharge protocol, commonly referred to as an asymmetric charge-discharge protocol.[16–18] For instance, Louli et al. have elucidated that during high-rate discharge, the development of a Li^+ concentration gradient enables an increased current density at the tips of the Li deposits.[17] This phenomenon leads to preferential stripping from the tips, effectively removing nonuniform deposits. Consequently, an anodeless LMB exhibits a longer cycle life due to higher CE achieved at relatively higher discharge currents. In contrast, Zeng et al. present a different perspective, demonstrating that high-rate discharge creates a transient high concentration Li^+ layer in close proximity to the Li metal surface.[16] This high concentration Li^+ layer coordinates with large number of solvent molecules, reducing the number of free solvents available for decomposition at the Li metal surface, thus minimizing the production of parasitic products. According to Zeng et al., longer cycle life observed during high-

[a] Dr. A. Dutta, E. Mizuki, Dr. S. Matsuda
Center for Green Research on Energy and Environmental Materials
National Institute for Materials Science
1-1 Namiki, Tsukuba, Ibaraki 305-0044 (Japan)
E-mail: DUTTA.arghya@nims.go.jp
MATSUDA.Shoichi@nims.go.jp

[b] E. Mizuki, Dr. S. Matsuda
NIMS-SoftBank Advanced Technologies Development Center
National Institute for Materials Science
1-1 Namiki, Tsukuba, Ibaraki 305-0044 (Japan)

[c] Dr. S. Matsuda
Center for Advanced Battery Collaboration
National Institute for Materials Science
1-1 Namiki, Tsukuba, Ibaraki 305-0044 (Japan)

Supporting information for this article is available on the WWW under https://doi.org/10.1002/batt.202300309

rate discharge stems from the mitigation of parasitic electrolyte decomposition and formation of a stable SEI layer. Therefore, despite the demonstrated advantages of high-rate discharge in improving LMB performance, the precise underlying mechanism remains elusive. These contrasting findings highlight the necessity of further investigation to unravel the underlying mechanisms governing the observed effects.

Based on these research backgrounds, this study delves into investigating the impact of discharging rate on the degradation of the Li metal electrode in pouch-type cells with a cell-level energy density exceeding 350 Wh kg^{-1}. To achieve this, appropriate technological parameters such as lean electrolyte and a high areal capacity were meticulously fine-tuned. In high-energy-density cell designs, the Li metal electrode is typically susceptible to damage during the cell disassembling process. Therefore, non-destructive techniques play a crucial role in acquiring quantitative information pertaining to the degradation of the Li metal electrode accurately. In this study, X-ray computed tomography (XCT) analysis was employed as an effective non-destructive analytical technique for obtaining three-dimensional structural information without causing damage to the samples. The XCT results revealed significant volume expansion of the Li electrode throughout repeated charge/discharge cycles. Nevertheless, under high-rate discharge conditions, the undesired volume expansion was significantly mitigated. While several studies have explored the use of XCT techniques for analyzing the reaction mechanisms of Li metal deposition/dissolution processes,[19–27] to our knowledge, the applications of XCT technology for high-energy-density pouch-type LMBs are limited.

Results and Discussion

In order to achieve high specific-energy beyond LIBs, a high-capacity as well as high-voltage positive electrode, thin Li-metal foil and lean electrolyte are necessary in a practical LMB.[1,2] In the present study, we fabricated LMBs with high areal-capacity NMC811 positive electrode (30 mg cm^{-2}, 6.6 mAh cm^{-2}), thin lithium metal negative electrode (50 μm, 9.8 mAh cm^{-2}, negative/positive capacity ratio (N/P ratio) < 1.5), and a lean electrolyte condition (10 μL cm^{-2} or $\approx$2 g Ah^{-1}). 4 M Lithium bis(fluorosulfonyl)imide (LiFSI) in dimethoxy ethane (DME) was utilized as the electrolyte. We present a schematic representation of the pouch cells employed in this study in Figure S1. The pie chart in Figure S2 shows the weight distribution of all the cell components used in this pouch cell. Besides, the variation of specific energy with electrolyte amount for different mass loading and 50 μm thick Li is shown in Figure S3. Notably, the cell employed in our study, marked by the red asterisk, exhibits a remarkably high specific energy exceeding 350 Wh kg^{-2}. Consequently, the results presented herein hold significant industrial and academic implications.

At first, we investigated the effect of discharging rate on the performance of LMBs. Fabricated LMB cells were charged at a relatively low current density (0.6 mA cm^{-2}) and subsequently discharged at both low rate (0.6 mA cm^{-2}) and high rate (3.0 mA cm^{-2}) conditions. Figure 1(a and b) presents the galvanostatic charge/discharge curves for selected cycles. The highest cycle number depicted in both Figure 1(a) and (b) corresponds to the cycle beyond which the specific capacity (Q) of the cell drops below 80% of its initial capacity. The results unequivocally demonstrate that discharging at a high rate leads to a threefold improvement in cycle-life, as indicated by capacity retention, compared to discharging at a low rate. Figure 1(c) illustrates the variation of capacity of the cells over successive cycles up to 80% capacity retention. One clear observation from Figure 1(a and b) and the voltage-time curves presented in Figure S4 is that cell failure is not attributed to a short-circuit. Instead, an increase in voltage polarization is observed towards the end cycles in both cases. This rise in voltage polarization can be ascribed to the increase in internal resistance of the cell. To complement these findings, we performed the electrochemical impedance analysis of cells after 20th cycle (Figure 1d). The results clearly reveal that the cell subjected to high-rate discharge exhibits marginally lower interfacial (Figure 1e) and charge transfer (Figure 1f) resistances. These findings unquestionably emphasize the influence of high-rate discharge in lowering impedance increase within the cell, thereby enhancing its cycle-life.

We also investigated the effect of discharging rate on the performance of LMBs under high charging rate condition (3.0 mA cm^{-2}). The galvanostatic voltage profiles obtained from selected cycles of these cells are displayed in Figure 2(a) and (b), respectively. Similar to Figure 1(a and b), the highest cycle number depicted in both Figure 2(a) and (b) corresponds to the cycle beyond which the specific capacity of the cell drops below 80% of its initial capacity. Significantly, it is noteworthy that the positive impact of high-rate discharging on enhancing the cycle life was observed even under high-rate charging conditions. Figure 2(c) illustrates the variation of capacity with cycle number for the cells. It is observed that the capacities of the cells charged at high rate are lower compared to those charged at low rate. It is quite understandable that at higher rates of charge, the cell experiences higher kinetic and Li^+-diffusion polarizations, causing it to reach the upper cut-off potential earlier compared to cells charged at lower rates. One notable observation depicted in Figure 2(c) is that, under low-rate discharge condition, the capacity of the cell does not exhibit a gradual decay. Instead, the cell experiences a sudden failure after 59 cycles and shows negligible capacity in the 60th cycle as shown in Figure S5. This phenomenon is corroborated by the voltage profiles presented in Figures 2(a) and S6, which indicate significant overcharging of the cell beyond the 50th cycle, with particularly pronounced overcharging observed from the 55th to the 59th cycles. Such overcharging and the subsequent abrupt cell failure can be attributed to a short-circuit within the cell. Unlike the cell subjected to the low-rate discharging, the capacity fading in the cell cycled under the high-rate discharging is more gradual, as evident from Figure 2(c). Moreover, the voltage profile in Figure 2(b) demonstrates a rapid increase in voltage polarization of the cell during end-cycles. Therefore, it can be inferred that the capacity fading observed in the cell subjected to the high-rate discharging is attributed to an

Research Article
doi.org/10.1002/batt.202300309
Chemistry Europe
European Chemical Societies Publishing

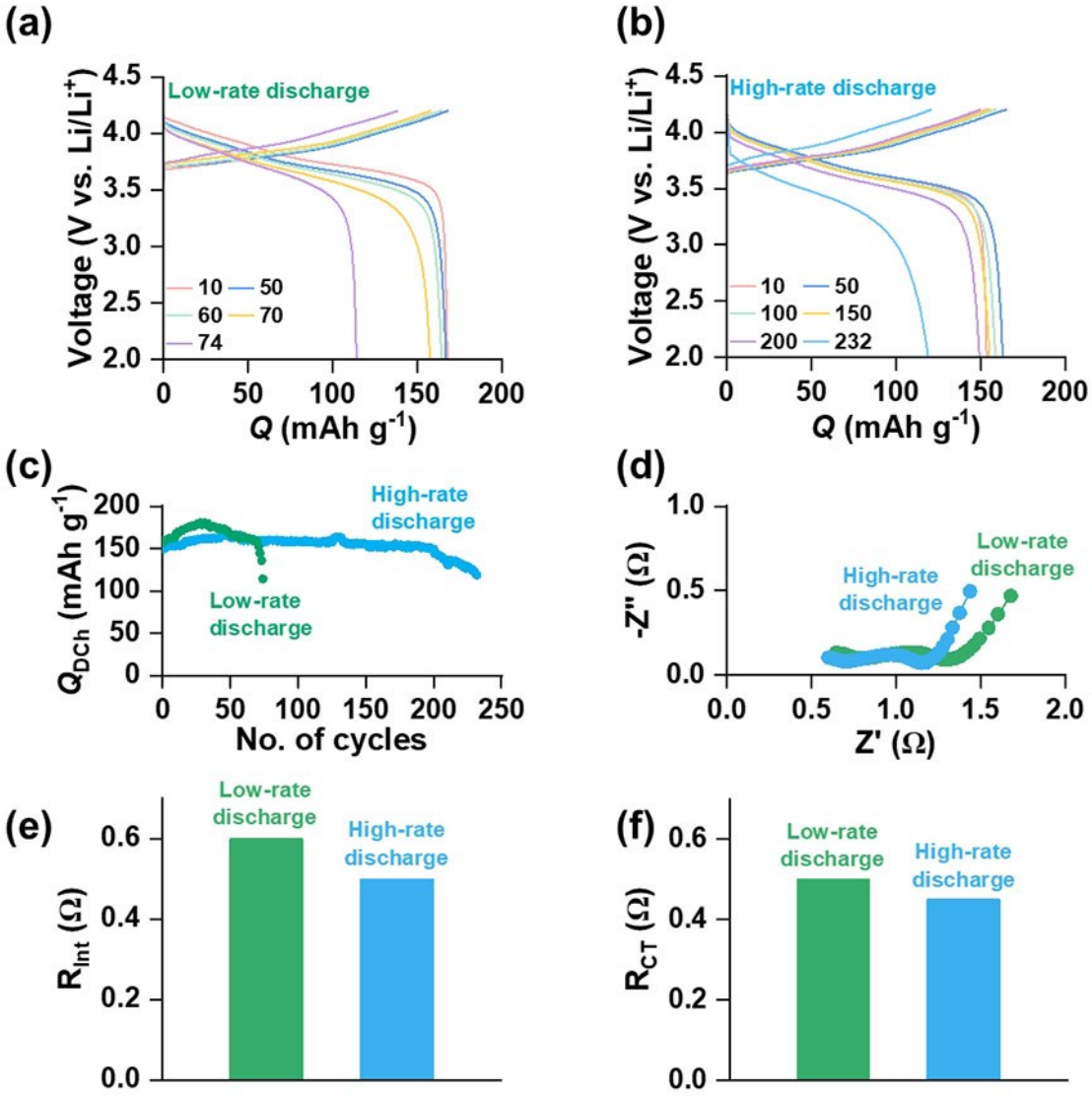

Figure 1. Discharge rate dependency at low-rate charging: a) voltage profile at selected cycles for 0.6 mA cm^{-2} charge and 0.6 mA cm^{-2} discharge, b) voltage profile at selected cycles for 0.6 mA cm^{-2} charge and 3.0 mA cm^{-2} discharge, c) capacity vs. cycle, d) electrochemical impedance spectra, e) interfacial resistance and f) charge transfer resistance of different cells after 20th cycle.

increase in cell impedance. Figure 2(d–f) demonstrates the results of electrochemical impedance analysis of the cell after 20th cycle, indicating that the cell discharged at a high-rate exhibits reduced interfacial and charge transfer resistances in comparison to the cell discharged at a low rate.

It also should be noted that the cell discharged at high-rate experienced several instances of soft-short-circuits during the cycling process. For instance, as depicted in Figure S7, the cell encountered a short-circuit as early as at the 7th cycle. Additionally, there were occurrences of soft-short-circuits at approximately 20 and 50 cycles. Nonetheless, the cell managed to recover from these short-circuits during subsequent cycles of stripping and plating by eliminating the Li center responsible for the short-circuit. In short, the results presented in Figures 1 and 2 confirm that high-rate discharging provides longer cycle-life by delaying both the impedance growth and short-circuit in the cell. Uneven deposition/dissolution leading to electrically disconnected Li, which is often termed as dead Li, and continuous accumulation of insulating SEI residues due to reaction of Li-metal with the electrolyte usually increase the impedance of the cell.[28,29] On the contrary, short-circuit in Li-metal cells occurs due to deposition of dendritic Li that penetrates the separator.[21,30] Therefore, observing the morphological evolution of the Li-metal electrode over the cycles can provide more precise understanding about the failure modes of the cells.

Subsequently, to gain a comprehensive understanding of the degradation phenomenon of the Li metal electrode, we conducted XCT analysis on the pouch cells after specific cycles. Despite our attempts to conduct a series of standard ex situ analyses, the Li metal electrodes were prone to damage during the cell disassembling process after repeated charge/discharge

Research Article
doi.org/10.1002/batt.202300309
Chemistry Europe
European Chemical Societies Publishing

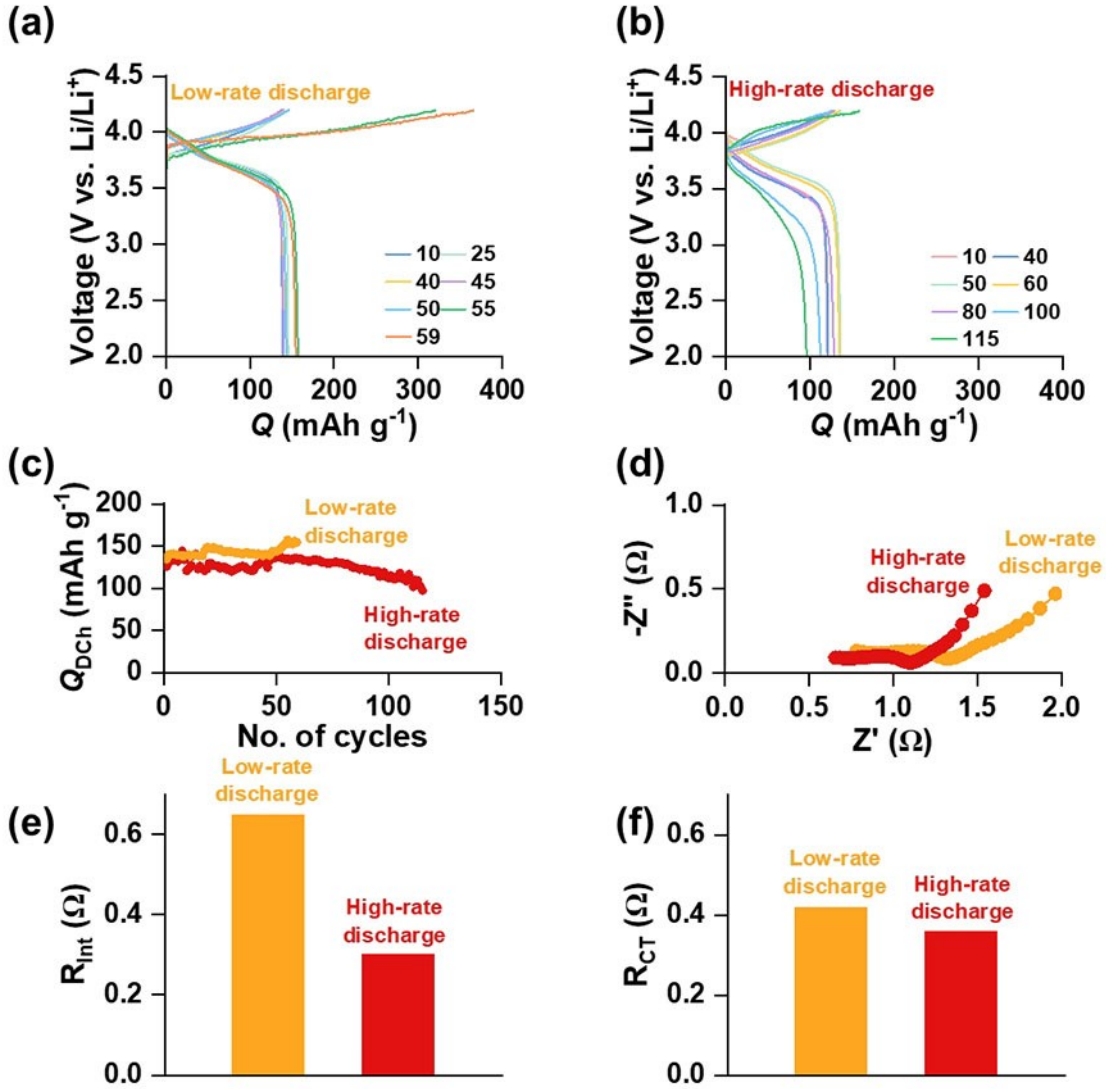

Figure 2. Discharge rate dependency at high-rate charging: a) voltage profile at selected cycles for 3.0 mA cm^{-2} charge and 0.6 mA cm^{-2} discharge, b) voltage profile at selected cycles for 3.0 mA cm^{-2} charge and 3.0 mA cm^{-2} discharge, c) capacity vs. cycle, d) electrochemical impedance spectra, e) interfacial resistance and f) charge transfer resistance of different cells after 20th cycle.

cycles. In this regard, the advantage of employing XCT is its non-destructive nature, allowing for analysis without causing damage to the cell or electrodes throughout the cycling process.[20] Notably, XCT analysis provides valuable information regarding the physical evolution of Li metal electrodes and facilitates the estimation of changes in their thickness. While previous studies have utilized XCT to analyze Li metal electrodes, a comprehensive analysis of high energy density Li|NMC811 cells at the practical level has not been conducted yet.

We first focused on the LMB cells cycled with low-rate charge conditions. As depicted in Figures S8(a) and 3(a), the initial thickness of the 50 μm Li-metal electrode increases to ≈90 μm after 10 cycles and further to ≈112 μm after 20 cycles of plating/stripping in the low-rate discharging condition. Conversely, in the case of the high-rate discharging, in Figure S8b and Figure 3b, the electrode thickness increases to 72 and 75 μm after 10 and 20 cycles respectively. The obtained results unequivocally demonstrate that the Li metal electrode undergoes significant growth, exceeding 120% after 20 cycles when subjected to low-rate discharge. In stark contrast, under high-rate discharge, the observed growth is approximately 50% (Figure 3c). Therefore, it is clear that thickness growth of the Li electrode is substantially suppressed when the cell is discharged at a relatively higher rate.

We also carried out similar XCT analyses of the cells charged at higher rate condition. Notably, a significant increase in the negative electrode thickness is observed for the low-rate discharging condition in Figures S8(c) and 3(d). After undergoing 10 cycles, in Figure S8c, the thickness of the sample exhibits a remarkable increase of more than 120% relative to its initial value, reaching approximately 115 μm. Progressive exac-

Research Article
doi.org/10.1002/batt.202300309
Chemistry Europe
European Chemical Societies Publishing

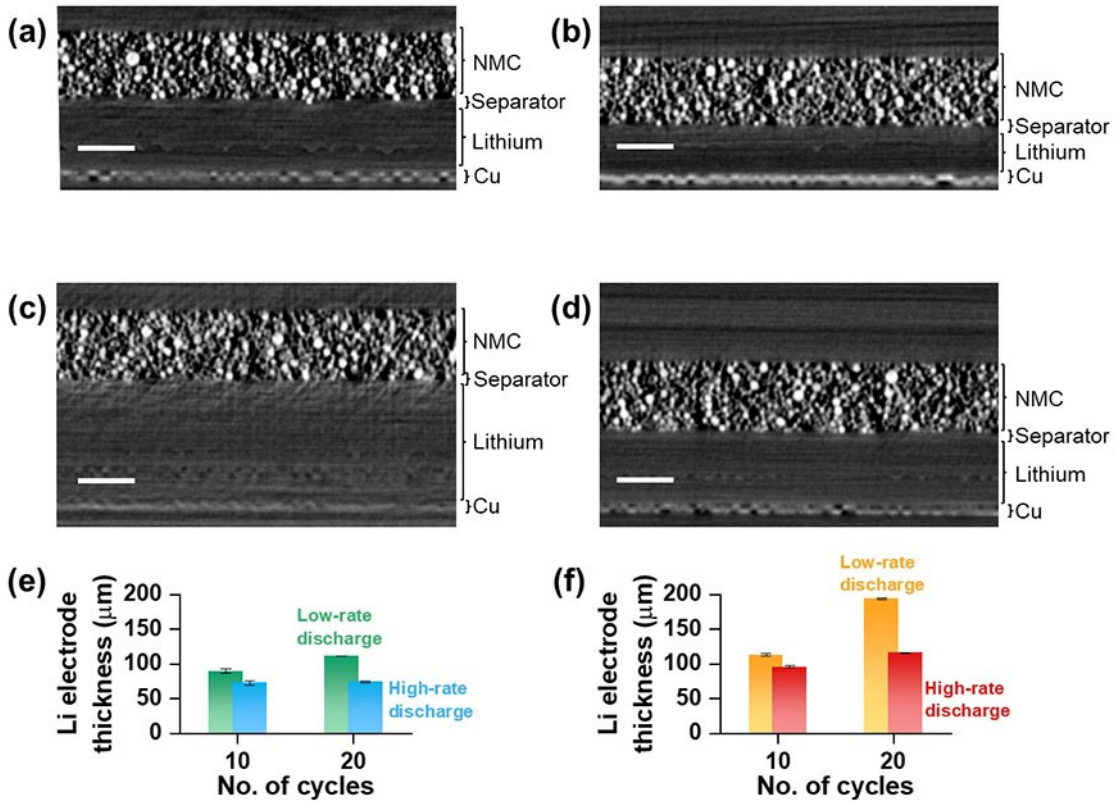

Figure 3. Cross-section XCT images of pouch cell. a) After 20th cycle at low-rate discharge and b) high-rate discharge under low-rate charge condition. c) After 20th cycle at low-rate discharge and d) high-rate discharge under high-rate charge condition. Scale bars are 100 μm. Quantitative comparison of effect of discharge rate on the thickness of the Li electrodes at e) low-rate charge and (f) high-rate charge condition.

erbation of electrode swelling is observed to persist at a more pronounced level, leading to significant changes in thickness. Particularly, after completing 20 cycles, a noteworthy growth phenomenon is witnessed in Figure 3(d), resulting in a substantial enhancement of the thickness to approximately 195 μm. On the other hand, the cell cycled at the high-rate discharging condition, shows a slightly smaller increase in the thickness of the Li-metal foil, as depicted in Figures S8(d) and 3(e). The thickness of the Li electrode measures ≈96 μm and ≈116 μm after 10 and 20 cycles, respectively (Figure 3f). These results clearly reveal that the suppression of volume change of electrode under high-rate discharge condition is a universal phenomenon regardless of the charging rate.

The magnified cross-sectional XCT image and selected slice images of the Li electrode in the surface direction at different layers of the Li metal electrode obtained at low-rate charging condition are shown in Figure 4. Regardless of the discharge-rate, there can be seen the three-layered structure in the Li metal electrode, (i) the bottom layer attached to Cu foil (Figure 4d and h), (ii) the middle layer, which is highlighted by the white dashed line (Figure 4c and 4g), and (iii) the top layer located near to the separator (Figure 4b and 4f). It should be noted that the XCT imaging was conducted under discharged conditions (0% state of charge), following the removal of Li from the negative electrode. Consequently, it is anticipated that freshly deposited Li from the prior charging, which had been in electrical contact, might have been stripped away.

At low-rate discharge condition, the XCT images revealed that the thicknesses of the bottom layer, middle layer and top layer are 40 μm, 20 μm and 60 μm, respectively (Figure 4a). Considering the fact that the initial thickness of Li metal electrode was 50 μm, the bottom layer can be assigned as the unused metallic Li foil. Recent analytical studies for degradation mechanism of Li metal electrode under lean electrolyte condition revealed the accumulation of the SEI compounds and electrically isolated dead Li particles between the unused metallic Li foil and separator.[20,29] Thus, the middle layer and top layer observed in this study can be assigned as the composite of SEI compounds and deal Li. Notably, the slice XCT image revealed the formation of several tens of micrometer sized particles in the middle layer (Figure 4c), indicating that the dead Li was main component in the middle layer. In contrast, in the top layer, the XCT image do not show clear structure in the electrode. Thus, the SEI compounds are considered as main component in top layer.

At high-rate discharge condition, the XCT images revealed that the thicknesses of the bottom layer, middle layer and top layer are 40 μm, 20 μm and 30 μm, respectively (Figure 4e). Although the thicknesses of both the bottom layer and the middle layer are mostly same with that observed at low-rate

Research Article
doi.org/10.1002/batt.202300309
Chemistry Europe
European Chemical Societies Publishing

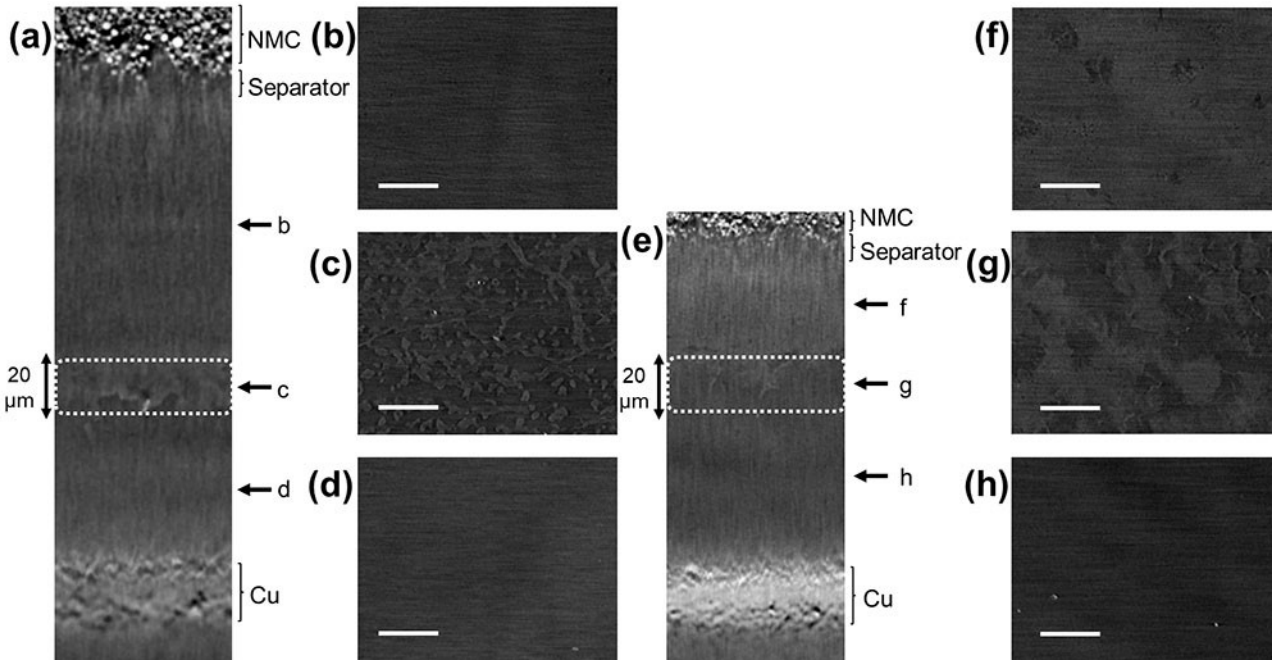

Figure 4. Magnified cross-section XCT images of pouch cell. a) After 20th cycle at low-rate discharge and e) high-rate discharge under low-rate charge condition. White dotted lines indicate the position of middle layer. b–d) XCT slice images in the surface direction from the same cells and the particular layers of image acquisition is indicated in (a). f–h) XCT slice images in the surface direction from the same cells and the particular layers of image acquisition is indicated in (e). Scale bars are 200 μm.

discharge condition, there can be clear differences in the thickness of the top layer. In addition, the slice XCT images of the middle and top layers revealed the formation of hundreds of micrometers sized large structure in the middle layer and top layer. These results clearly reveal the large impact of discharge-rate on the morphology of Li metal electrodes. In particular, difference in top layer is considered to be the physicochemical origin of positive effect of high-rate discharging for suppressing volume expansion of Li metal electrodes.

The magnified cross sectional XCT images of the Li electrode obtained at high-rate charging condition are also shown in Figure S9. Even in this case, regardless of the discharge rate, the three-layer structures were observed. Notably, in high-rate charge condition, the increase of thickness in top layer is more prominent compared to the case in low-rate charge conditions. The slice XCT images of the Li electrode obtained at high-rate charging condition are also shown in Figure S9. Even in this case, there can be seen the clear difference in the thickness of the top layer of the electrodes from low-rate and high-rate discharge conditions. Notably, a thinner top layer was observed at the high-rate discharge conditions. These results suggest that the volume expansion of the top layer in Li metal electrode can be largely suppressed under high-rate discharge.

Here let us summarize the effect of current density during discharge process on the degradation mechanism of Li metal electrode under high areal capacity and lean electrolyte condition. During repeated charge/discharge cycles, undesired side reaction between Li metal and the organic electrolyte gives rise to the formation of an electrically insulating SEI layer on the electrode surface. In addition, electrically isolated Li metal deposits are also formed. These side products accumulate on the electrode. Due to the relatively low electrolyte content ($\approx 2\ g\ Ah^{-1}$) in the cells, the entrapment of electrolyte within the electrode pores leads to a shortage of electrolyte.[31,32] Consequently, this electrolyte shortage exacerbates impedance growth and results in an inhomogeneous distribution of current within the electrode. The series of XCT results obtained in the present study reveal that cell failure attributed to impedance growth originated in the increase in electrode thickness. Notably, at high-rate discharge condition, the stripping of Li-particles proceeds at the tip/corner of the deposit where the equipotential lines are highly concentrated.[33] As a result, Li stripping reaction at high-rate reduces inhomogeneity, which suppresses the formation of both dendritic and electrically disconnected dead Li. These effects results in the suppression of volume expansion of the electrode under high-rate discharge conditions, leading to a smaller rise in impedance within the cell. This phenomenon is the fundamental reason behind the extended cycle life. In contrast, at low-rate discharge condition, a homogeneous distribution of the equipotential lines around the particles leads to an isotropic stripping from any location of the particles.[32] Therefore, thinning of the particles at some curved or necking regions can lead to fragmentation of the particles producing dead Li, resulting in the undesired volume expansion of the electrode.

In the present study, by using non-destructive XCT technique, we demonstrated that the volume expansion of Li metal electrode is one of the key phenomena for explaining the improvement of cycle life under high-rate discharge condition.

However, for the comprehensive understanding of the cell degradation mechanism, the studies for NMC positive electrode side are also crucial, including the decay rate and the utilization rate of NMC positive electrode at different current densities. Further study regarding the understanding of complicated electro/chemical reaction in Li metal based rechargeable batteries is now on-going in our laboratory.

Conclusions

In this study, we conducted an investigation of the benefits of high-rate discharge current densities in Li metal-based rechargeable batteries with cell level high energy density condition. By the use of non-destructive ex situ XCT technique, the evolution of the Li electrodes was investigated, revealing that the Li electrode undergoes volume expansion during cycling, attributed to the deposition of non-compact Li and the accumulation of SEI compounds. The cumulative effects of these electrically insulating SEI deposits and the entrapment of electrolyte within the expanded electrode contribute to an increase in cell impedance, which leads to cell failure. This aggravation of volume expansion and impedance growth is more pronounced at higher charging currents due to the deposition of smaller Li particles, which leads to a larger surface area in contact with the electrolyte, resulting in increased SEI product accumulation. Nevertheless, the XCT results presented here provide a clear evidence that high-rate discharge suppresses the volume expansion of Li electrode. While the benefits of faster discharge have been previously reported, our study offers physicochemical insight for this phenomenon. In particular, the methodology demonstrated in the present study also can be applicable even for multi-layer stacked pouch cells. We believe that the results presented in this study provide crucial insights for achieving high energy density LMB with longer cycle life.

Supporting Information

Experimental details, schematic representation of the pouch cell, pie chart showing weight distribution of cell components, variation of specific-energy with electrolyte volume, additional galvanostatic charge/discharge curves, electrochemical impedance data and additional XCT images are provided in the Supporting Information.

Acknowledgements

The present work was partially supported by JST COI-NEXT Grant Number JPMJPF2016. This work also received support from the National Institute for Materials Science (NIMS) Battery Research Platform.

Conflict of Interests

The authors declare no conflict of interest.

Data Availability Statement

The data that support the findings of this study are available from the corresponding author upon reasonable request.

Keywords: lithium metal battery · high-capacity battery · failure analysis · charge-discharge rate · battery diagnosis

[1] X. Ren, L. Zou, X. Cao, M. H. Engelhard, W. Liu, S. D. Burton, H. Lee, C. Niu, B. E. Matthews, Z. Zhu, C. Wang, B. W. Arey, J. Xiao, J. Liu, J.-G. Zhang, W. Xu, *Joule* **2019**, *3*, 1662.
[2] J. Liu, Z. Bao, Y. Cui, E. J. Dufek, J. B. Goodenough, P. Khalifah, Q. Li, B. Y. Liaw, P. Liu, A. Manthiram, Y. S. Meng, V. R. Subramanian, M. F. Toney, V. V. Viswanathan, M. S. Whittingham, J. Xiao, W. Xu, J. Yang, X.-Q. Yang, J.-G. Zhang, *Nat. Energy* **2019**, *4*, 180.
[3] C. Zhu, C. Sun, R. Li, S. Weng, L. Fan, X. Wang, L. Chen, M. Noked, X. Fan, *ACS Energy Lett.* **2022**, *7*, 1338.
[4] G.-X. Li, H. Jiang, R. Kou, D. Wang, A. Nguyen, M. Liao, P. Shi, A. Silver, D. Wang, *ACS Energy Lett.* **2022**, *7*, 2282.
[5] X.-Q. Zhang, T. Li, B.-Q. Li, R. Zhang, P. Shi, C. Yan, J.-Q. Huang, Q. Zhang, *Angew. Chem. Int. Ed.* **2020**, *59*, 3252.
[6] R. Weber, M. Genovese, A. J. Louli, S. Hames, C. Martin, I. G. Hill, J. R. Dahn, *Nat. Energy* **2019**, *4*, 683.
[7] S. Yuan, T. Kong, Y. Zhang, P. Dong, Y. Zhang, X. Dong, Y. Wang, Y. Xia, *Angew. Chem. Int. Ed.* **2021**, *60*, 25624.
[8] H. Wu, H. Jia, C. Wang, J.-G. Zhang, W. Xu, *Adv. Energy Mater.* **2021**, *11*, 2003092.
[9] Y. Zhang, Y. Wu, H. Li, J. Chen, D. Lei, C. Wang, *Nat. Commun.* **2022**, *13*, 1297.
[10] S. Chen, J. Zheng, D. Mei, K. S. Han, M. H. Engelhard, W. Zhao, W. Xu, J. Liu, J.-G. Zhang, *Adv. Mater.* **2018**, *30*, 1706102.
[11] S. Chen, J. Zheng, L. Yu, X. Ren, M. H. Engelhard, C. Niu, H. Lee, W. Xu, J. Xiao, J. Liu, J.-G. Zhang, *Joule* **2018**, *2*, 1548.
[12] K. Shi, A. Dutta, Y. Hao, M. Zhu, L. He, Y. Pan, X. Xin, L.-F. Huang, X. Yao, J. Wu, *Adv. Funct. Mater.* **2022**, *32*, 2203652.
[13] W. Beichel, J. Skrotzki, P. Klose, C. Njel, B. Butschke, S. Burger, L. Liu, R. Thomann, Y. Thomann, D. Biro, S. Thiele, I. Krossing, *Batteries & Supercaps* **2022**, *5*, e202100347.
[14] D. Kang, M. Xiao, J. P. Lemmon, *Batteries & Supercaps* **2021**, *4*, 445.
[15] C. Fang, B. Lu, G. Pawar, M. Zhang, D. Cheng, S. Chen, M. Ceja, J.-M. Doux, H. Musrock, M. Cai, B. Liaw, Y. S. Meng, *Nat. Energy* **2021**, *6*, 987.
[16] J. Zheng, P. Yan, D. Mei, M. H. Engelhard, S. S. Cartmell, B. J. Polzin, C. Wang, J.-G. Zhang, W. Xu, *Adv. Energy Mater.* **2016**, *6*, 1502151.
[17] A. J. Louli, M. Coon, M. Genovese, J. deGooyer, A. Eldesoky, J. R. Dahn, *J. Electrochem. Soc.* **2021**, *168*, 20515.
[18] J. Qian, B. D. Adams, J. Zheng, W. Xu, W. A. Henderson, J. Wang, M. E. Bowden, S. Xu, J. Hu, J.-G. Zhang, *Adv. Funct. Mater.* **2016**, *26*, 7094.
[19] K. J. Harry, D. T. Hallinan, D. Y. Parkinson, A. A. MacDowell, N. P. Balsara, *Nat. Mater.* **2014**, *13*, 69.
[20] R. Tamate, S. Matsuda, *ACS Appl. Energ. Mater.* **2023**, *6*, 573.
[21] F. Sun, R. Moroni, K. Dong, H. Markötter, D. Zhou, A. Hilger, L. Zielke, R. Zengerle, S. Thiele, J. Banhart, I. Manke, *ACS Energy Lett.* **2017**, *2*, 94.
[22] S. Frisco, D. X. Liu, A. Kumar, J. F. Whitacre, C. T. Love, K. E. Swider-Lyons, S. Litster, *ACS Appl. Mater. Interfaces* **2017**, *9*, 18748.
[23] O. O. Taiwo, D. P. Finegan, J. M. Paz-Garcia, D. S. Eastwood, A. J. Bodey, C. Rau, S. A. Hall, D. J. L. Brett, P. D. Lee, P. R. Shearing, *Phys. Chem. Chem. Phys.* **2017**, *19*, 22111.
[24] G. Tonin, G. Vaughan, R. Bouchet, F. Alloin, M. Di Michiel, L. Boutafa, J.-F. Colin, C. Barchasz, *Sci. Rep.* **2017**, *7*, 2755.
[25] K. R. Adair, M. N. Banis, Y. Zhao, T. Bond, R. Li, X. Sun, *Adv. Mater.* **2020**, *32*, 2002550.
[26] F. Sun, L. Zielke, H. Markötter, A. Hilger, D. Zhou, R. Moroni, R. Zengerle, S. Thiele, J. Banhart, I. Manke, *ACS Nano* **2016**, *10*, 7990.

[27] A. J. Louli, A. Eldesoky, R. Weber, M. Genovese, M. Coon, J. deGooyer, Z. Deng, R. T. White, J. Lee, T. Rodgers, R. Petibon, S. Hy, S. J. H. Cheng, J. R. Dahn, *Nat. Energy* **2020**, *5*, 693.
[28] K.-H. Chen, K. N. Wood, E. Kazyak, W. S. LePage, A. L. Davis, A. J. Sanchez, N. P. Dasgupta, *J. Mater. Chem. A* **2017**, *5*, 11671.
[29] S. Matsuda, M. Ono, A. Myojin, *ACS Appl. Energ. Mater.* **2023**, *6*, 2524.
[30] K. L. Jungjohann, R. N. Gannon, S. Goriparti, S. J. Randolph, L. C. Merrill, D. C. Johnson, K. R. Zavadil, S. J. Harris, K. L. Harrison, *ACS Energy Lett.* **2021**, *6*, 2138.
[31] C. Niu, H. Lee, S. Chen, Q. Li, J. Du, W. Xu, J.-G. Zhang, M. S. Whittingham, J. Xiao, J. Liu, *Nat. Energy* **2019**, *4*, 551.
[32] X. Duan, L. Wang, G. Li, X. Liu, M. Wan, J. Du, R. Zhan, W. Wang, Y. Li, S. Tu, Y. Shen, Z. W. Seh, L. Wang, Y. Sun, *Adv. Funct. Mater.* **2023**, *33*, 2210669.
[33] G. Yoon, S. Moon, G. Ceder, K. Kang, *Chem. Mater.* **2018**, *30*, 6769.

Manuscript received: July 12, 2023
Revised manuscript received: August 27, 2023
Accepted manuscript online: September 6, 2023
Version of record online: September 21, 2023